

# Observations of Momentum Transfer in the Upper Ocean: Did Ekman Get It Right?

Daniel L. Rudnick

Scripps Institution of Oceanography, La Jolla, California

**Abstract.** The first theory of wind-driven flow is that of Ekman, who assumed a uniform eddy viscosity and derived the velocity spiral that bears his name. Over the years, observations of wind stress and current have improved to the point that frictional momentum transfer in the upper ocean can be quantified. Observations of velocity spirals are reviewed to address such issues as the vertical structure and penetration of wind-driven momentum and the frequency dependence of momentum transfer. Observed response is more slab-like than the theoretical Ekman spiral. The penetration depth does not vary with frequency as Ekman theory predicts, suggesting regulation by the mixed layer. Wind-driven momentum penetrates beneath the mixed-layer base, into a stratified region dominated by inertial shear.

## Introduction

The first theory of the wind driven circulation is that of *Ekman* (1905), who assumed negligible horizontal gradients and a constant eddy viscosity to derive his famous spiral. Observational confirmation of the spiral was difficult to attain until the last twenty years when significant measurement problems and signal-to-noise issues were overcome. The purpose of this paper is to review simple Ekman theory and relevant observations. Of particular interest is the depth of penetration of momentum into the upper ocean.

## Spiral theory

A starting point is the linear horizontal momentum equation, neglecting horizontal gradients, and assuming a constant eddy viscosity:

$$\frac{\partial u}{\partial t} + i f u = \nu \frac{\partial^2 u}{\partial z^2}. \quad (1)$$

Here,  $u$  is complex, with its real part being eastward velocity and imaginary part northward velocity,  $f$  is the Coriolis parameter, and  $\nu$  is the eddy viscosity. If the geocentric acceleration  $A$  is defined as the lhs of (1), and a solution of the form

$$A(z, t) = A(z, t) e^{i \omega t} \quad (2)$$

is assumed for rotary frequency  $\omega$ , the solution is

$$A(z) = A_0 \exp \left[ (1 \pm i) \left( \frac{|f + \omega|}{2\nu} \right)^{1/2} z \right]. \quad (3)$$

The surface geocentric acceleration  $A_0$  is determined by the stress boundary condition to be

$$A_0 = (1 \pm i) \frac{\tau_0}{\rho} \left( \frac{|f + \omega|}{2\nu} \right)^{1/2}. \quad (4)$$

The familiar Ekman spiral (Fig. 1) decays with depth and rotates, with a length scale (Ekman depth) of  $\sqrt{2\nu/|f + \omega|}$ . As the solution is complex, it rotates cyclonically with depth for  $\omega > -f$ , and anticyclonically for  $\omega < -f$ . At the inertial frequency,  $\omega = -f$ ,  $A$  vanishes and resonant inertial motions are explicitly filtered.

The Ekman spiral is a standard item in textbooks on physical oceanography, so is quite well known. It is, at least, entertaining to point out a few facts that may be less trite. As reported by *Ekman* (1905), Nansen suggested the problem, having observed ice-drift. At the time, Ekman was a graduate student working under Bjerknes. Remarkably, Ekman “produced the theory of the Ekman spiral that very evening.” (*Munk*, 2002). Ekman developed a current meter specifically to observe the spiral, but was never successful. One of the most common criticisms of the Ekman spiral, that it relies on an assumption of a uniform eddy viscosity,

was anticipated: “It is obvious that [ $\nu$ ] cannot generally be regarded as a constant when the density of water is not uniform within the region considered” (Ekman, 1905). Finally, Ekman considered an eddy viscosity dependent on shear in his 1905 work, and found insignificant differences from the constant eddy viscosity solution.

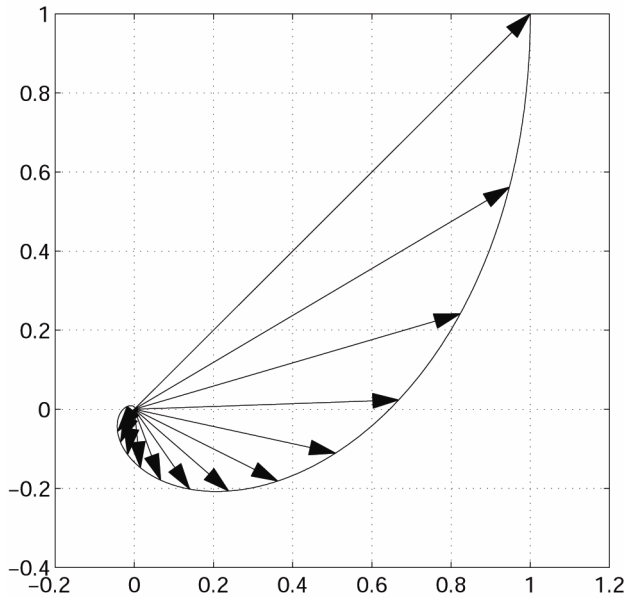


**Figure 1.** The steady Ekman spiral of geocentric acceleration. Arrows are plotted at increments of one-fourth the Ekman depth.

### Early observations of the spiral

The difficulty of measuring currents in the surface layer of the ocean limited early observations of wind-driven flow. A notable exception is *Hunkins* (1966), who observed current by lowering a drogue from an ice floe and measuring the wire angle. As a harbinger of methods to follow, Hunkins averaged over periods of relatively steady wind velocity to produce an average spiral (Fig. 2). Fitting the steady Ekman solution resulted in an Ekman depth of 18 m and an eddy viscosity of  $2.4 \times 10^{-3} \text{ m}^2 \text{ s}^{-1}$ . Hunkins claim that this was “apparently the first detailed confirmation of the Ekman spiral in deep waters” seems valid.

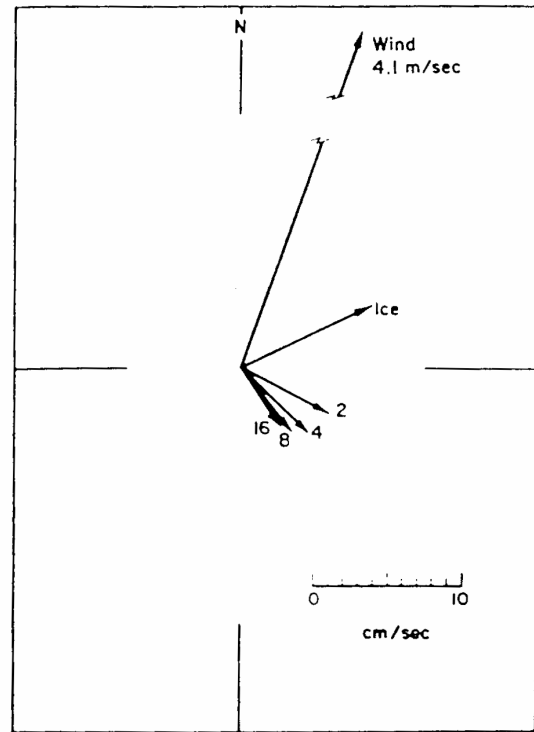


**Figure 2.** From *Hunkins* (1966), the wind-driven velocity spiral as measured using a drogue lowered from an ice floe. Numbers give depth in meters. The current is averaged over several measurement periods of 10-20 minute duration.

### Modern observations of the spiral

Verification of Ekman dynamics was made possible starting around 1980 with the development of robust surface moorings and improved current meters. The surface mooring provided a platform for simultaneous measurement of wind and current, though the platform was far from stable in an upper ocean dominated by surface waves. The Vector Measuring Current Meter (VMCM) was specifically designed to measure currents on a surface mooring subject to high-frequency oscillations, as by surface waves (*Weller and Davis*, 1980). The Acoustic Doppler Current Profiler (ADCP) has seen increasing use to measure profiles of current. The ADCP provides perhaps the best measure of shear from a mooring.

Given accurate measurements of velocity, the observational challenge is the signal-to-noise problem. The desired signal, wind-driven velocity, is often less energetic than noise from a number of sources. Noise at low

frequencies is due to geostrophic flow. At higher frequencies, internal waves are a dominant source of variability. Free inertial motions contribute to the noise if the goal is to find the directly wind-forced flow. Finally, mooring motion can contaminate otherwise accurate measurements of velocity. These signal-to-noise issues have been largely addressed through appropriate data analysis.

The first modern observation of the Ekman spiral was obtained during MILE (*Davis et al.*, 1981a,b). A transfer function between geocentric acceleration and wind stress was used to identify the wind-driven flow. The linear statistical model was

$$\hat{A}(\omega, z) = a(\omega, z) \frac{\tau_0(\omega)}{\rho}, \quad (5)$$

where  $\hat{A}$  was the geocentric acceleration coherent with the wind stress  $\tau_0$ , and  $a$  was the transfer function in units of inverse meters. The transfer function was found by minimizing the mean-square difference between the modeled and the measured geocentric acceleration,

$$a = \rho \frac{\langle \tau_0^* A \rangle}{\langle \tau_0^* \tau_0 \rangle}, \quad (6)$$

where the angle brackets were an average over frequency bands, and the asterisk signifies a complex conjugate. For this analysis to be successful at isolating the frictional wind-driven flow, all other driving forces, such as those due to pressure gradients or mooring motion, must be incoherent with the wind stress. An advantage of analyzing geocentric acceleration rather than velocity is that free inertial motions are suppressed.

*Davis et al.* (1981b) estimated the transfer function  $a$  using 19-day records and averaging over neighboring moorings and depths. Real and imaginary parts of  $a$  were shown in five frequency bands as a function of depth (Fig. 3). The presentation was flawed in the sense that it was difficult to identify a spiral. However, the combination of a real part decaying with depth, and an imaginary part growing, did produce a spiral (as for the rightmost four panels in the figure). The observed spiral turned less than the theoretical spiral, thus the response was more slab-like. The depth of the response did not vary with frequency, again consistent with slab mixed-layer dynamics. A simple slab-mixed-layer model (*Niiler*, 1975) did a reasonable job of reproducing the observed spiral.

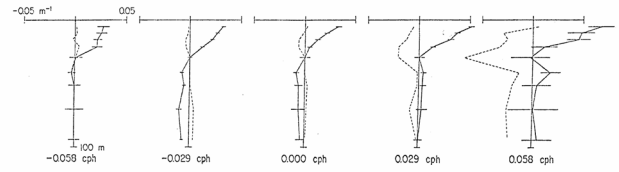


**Figure 3.** From *Davis et al.* (1981b), the transfer function  $a$  between wind stress and geocentric acceleration in five frequency bands. The solid lines are the real part of  $a$ , and the dashed lines are the imaginary part. Horizontal bars represent a one-standard-deviation error.

The ability of the analysis to isolate the wind-driven flow was tested by evaluating the Ekman transport relation, written as

$$\int_{-H}^0 a dz = 1, \quad (7)$$

where  $H$  is a depth at which stress vanishes. Before making this test, the average  $a$  deeper than 40 m was subtracted from the shallow  $a$ . This subtraction was necessary because pressure gradient driven flow was not filtered by the statistical analysis. The test (7) was carried out for each of the frequency bands of Fig. 3; observed transport agreed with theoretical transport to better than about 40% in magnitude and  $25^\circ$  in angle. That the comparison with theoretical Ekman transport was less than perfect for the MILE data was likely due to the relative shortness of the 19-day time series.

An influential demonstration of wind-driven flow in substantial agreement with the Ekman transport relation used 160-day time series from LOTUS (*Price et al.*, 1987). To isolate wind-driven flow, a clever technique termed “coherent ensemble averaging” was used wherein daily-average currents were rotated into a coordinate system in which the wind was in a constant direction before averaging. This procedure is equivalent to performing a regression between the current and a unit vector pointing in the direction of the wind stress,

$$\hat{u} = b \frac{\tau_0}{|\tau_0|}, \quad (8)$$

where  $b$  is the regression coefficient. The results again suggested a flattened spiral, indicative of a slab mixed layer (Fig. 4). The remarkable comparison with theoretical transport was taken to be a triumph of observational and analytical techniques rather than a confirmation of the Ekman transport relation. Because the Ekman transport relation does not rely on any particular

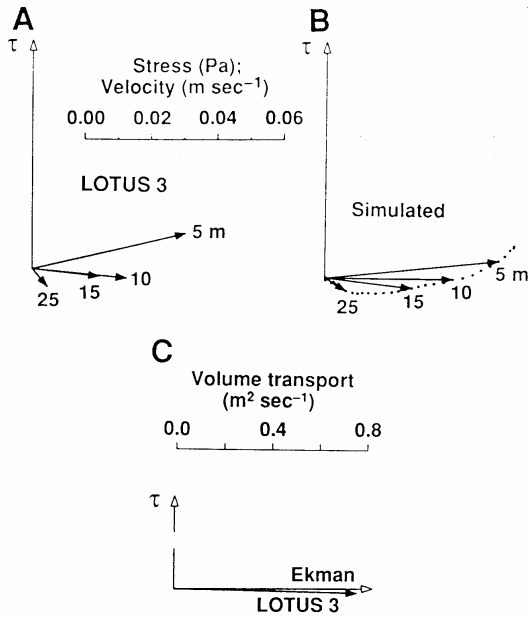


**Figure 4.** From *Price et al.* (1987), (A) the response produced through “coherent ensemble averaging,” or regressing current against wind direction. (B) Simulations from a one-dimensional mixed-layer model driven by the observed air-sea fluxes. (C) A comparison of observed and theoretical transport.

form for turbulent stress, only that it disappear at sufficient depth, it was regarded as unassailable. Even with 160-day records, a deep reference flow was again subtracted from shallower measurements to separate pressure-gradient-driven flow. A favorable comparison with a one-dimensional mixed-layer model (*Price et al.*, 1986) was another significant result of this important work.

The mystery of the deep flow coherent with wind stress was solved using observations from FASINEX (*Weller et al.*, 1991). The transfer function  $a$  was calculated in three subinertial frequency bands using 102-day records from five moorings (Fig. 5). Response coherent with the wind stress was found as deep as 1000 m at the lowest resolved frequencies. This response was attributed to pressure-gradient-driven flow caused by Ekman pumping. The evanescent response (*Philander*, 1978) had a vertical scale consistent with local forcing by weather systems of horizontal scale 700 km. As this geostrophic flow was coherent with local wind, no amount of averaging could have removed it, explaining the need to subtract a deep reference velocity. After subtraction of the geostrophic flow, the good agreement with theoretical transport mirrored that in previous works.

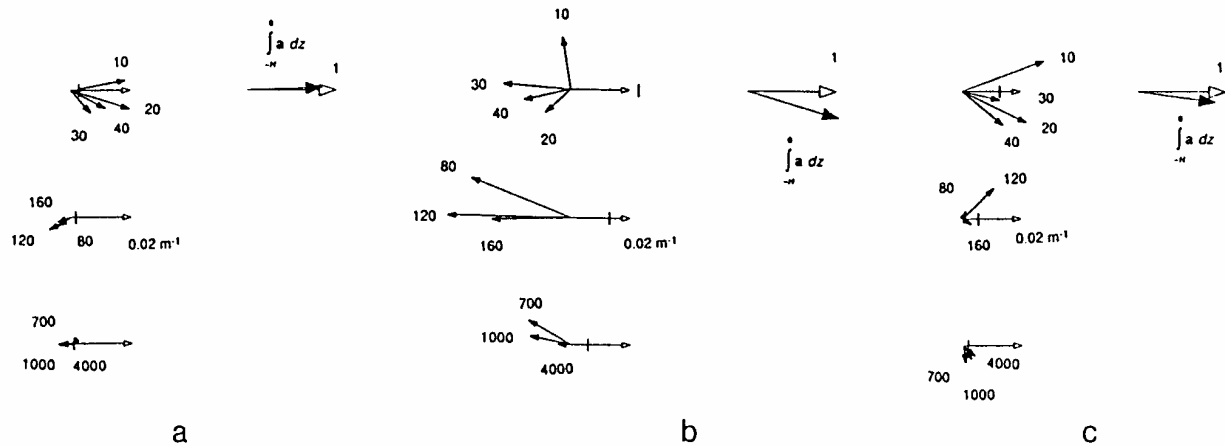


**Figure 5.** From *Weller et al.* (1991) the transfer function  $a$  between geocentric acceleration and wind stress in three bands: rotary periods between  $-1.5$  and  $-10$  days (a), between  $-10$  and  $10$  days (b), and between  $10$  and  $1.5$  days. Comparisons with theoretical transport are also shown.

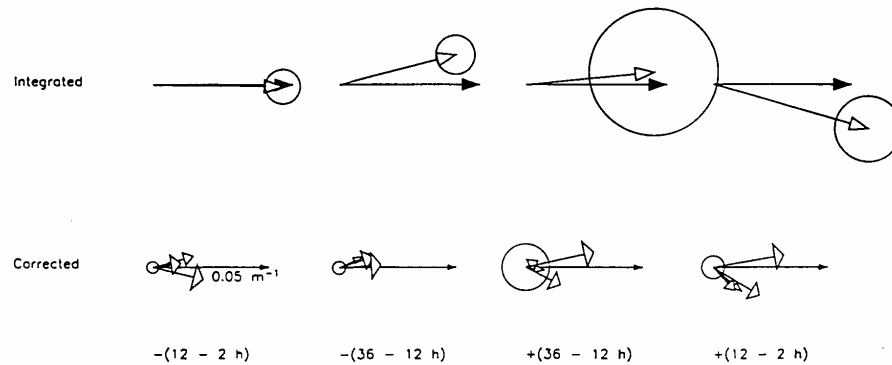


**Figure 6.** From *Rudnick and Weller* (1993), the transfer function between geocentric acceleration and wind stress, corrected for mooring motion (bottom row), and integrated (top row), in four frequency bands (columns). Circles indicate one-standard-deviation errors.

The Ekman spiral at superinertial frequencies was investigated using LOTUS and FASINEX data (*Rudnick and Weller*, 1993). Internal waves resided at these frequencies, contributing to the signal-to-noise problem. Because free internal waves were incoherent with local wind, sufficient averaging brought out the wind-driven flow. However, mooring motion was found to be a serious source of noise at high frequencies, as wind pushed the surface buoy. Wind-driven response on FASINEX surface moorings was identified down to 1000 m, and was strongest at the highest resolved frequencies (Nyquist 0.5 cph). However, subsurface moorings from LOTUS had no such response, thus implicating the mooring line as the mechanism of momentum transfer.

After correcting for the mooring motion, again by subtraction of the deep response, superinertial and near-inertial spirals were identified (Fig. 6). In agreement with theory, the spirals turned to the left for  $\omega < -f$ , and to the right for  $\omega > -f$ . Agreement with theory was apparent despite the poor signal-to-noise ratios. Long time series were essential to provide adequate degrees of freedom at these high frequencies.

To this point, all of the observations of Ekman spirals occurred in regions where the forcing was dominated by weather systems of several-day time scales. Spirals had been identified at a wide range of frequencies from lower than 1/10 cycles per day to 1/2 cycles per hour. However, a spiral at zero frequency had never been observed because the ratio of wind mean to fluctuating energy was always small. Off of Northern California, in contrast, winds after the spring transition are notably steady, allowing *Chereskin* (1995) to observe a steady spiral (Fig. 7). After subtraction of

a deep reference flow at 48 m, the transport agreed with theory to within 3% in magnitude and 4° in direction. Constant eddy viscosities of the order 0.01 m<sup>2</sup> s<sup>-1</sup> yielded the best fit with the theoretical spiral.

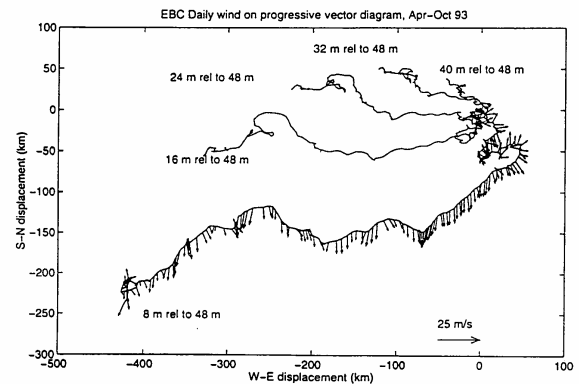


**Figure 7.** From *Chereskin* (1995), a progressive vector diagram using daily averaged currents relative to 48 m. Wind velocity is plotted along the shallowest displacement curve.

The SW Arabian Sea monsoon is famously steady. Observations from the Arabian Sea Experiment (*Weller et al.*, 2002) offer another realization of the steady transfer function. The current relative to 80 m averaged over the first 2.5 months of the SW monsoon shows the familiar, flattened spiral (Fig. 8). Integrating this spiral yields a transport within 1% in magnitude and 6° in direction of the theoretical value. A fit of the Ekman spiral solution produces an Ekman depth of 50 m and an eddy viscosity of 0.05 m<sup>2</sup> s<sup>-1</sup>.

Moored observations have proven unambiguously that a wind-forced velocity spiral exists. The spiral has been observed at time scales short enough to be in the internal wave frequency band, and as long as a few

months. The observed spiral turns less, and is thus more slab-like, than the theoretical Ekman spiral. The penetration depth of the observed spiral does not vary with frequency as does the theoretical spiral, suggesting the primacy of stratification in controlling the eddy viscosity. The idea of a stratified velocity spiral influenced by the mixed layer seems valid.

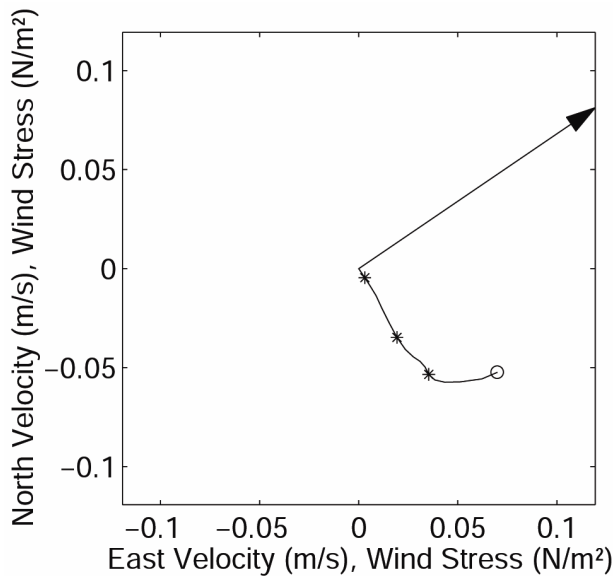


**Figure 8.** The velocity spiral averaged over May 1 – July 15, 1995 during the SW Arabian Sea monsoon. The solid line is average velocity relative to 80 m, at a resolution of 4 m (from a moored ADCP). The shallowest velocity, indicated with a circle, is at 8 m. Velocities at depths of 28, 48, and 68 m are marked with asterisks. The arrow is the mean wind stress over the same period.

### Effects of stratification

As anticipated by Ekman, stratification indeed affects the wind-driven velocity spiral. In fact, the models that have reproduced the observed spiral have had stratification as a fundamental component, primarily through a slab mixed layer. Hidden in many of these models is some sort of mixing in the stratified region beneath the mixed layer. As the slab mixed layer is the common feature of the models, this sub-mixed-layer mixing may be the key difference between models.

Observations suggest that wind-driven momentum penetrates below the mixed layer. For example, *Chereskin and Roemmich (1991)* used shipboard ADCP and hydrographic measurements to determine that wind-driven momentum penetrated as deep as twice the mixed-layer depth. Open questions are what

determines the depth of penetration, and what is an appropriate parameterization for this sub-mixed-layer turbulent momentum flux. Besides mixed-layer depth, relevant parameters include stratification and shear in the region beneath the mixed layer.

The penetration depth of wind-driven flow is examined using moored ADCP data from the Arabian Sea. Low-passed (168-hour) currents are integrated from the surface to the depth where the agreement with theoretical wind-driven transport is best. Consistent with previous studies, geostrophic flow is removed by subtracting the flow at this best depth. The observed transport is normalized by the Ekman transport so that perfect agreement would be indicated by a normalized transport of 1 at angle 0°. The result of this calculation is shown for the SW monsoon (Fig 9). Agreement with theory is reasonably good, except when the

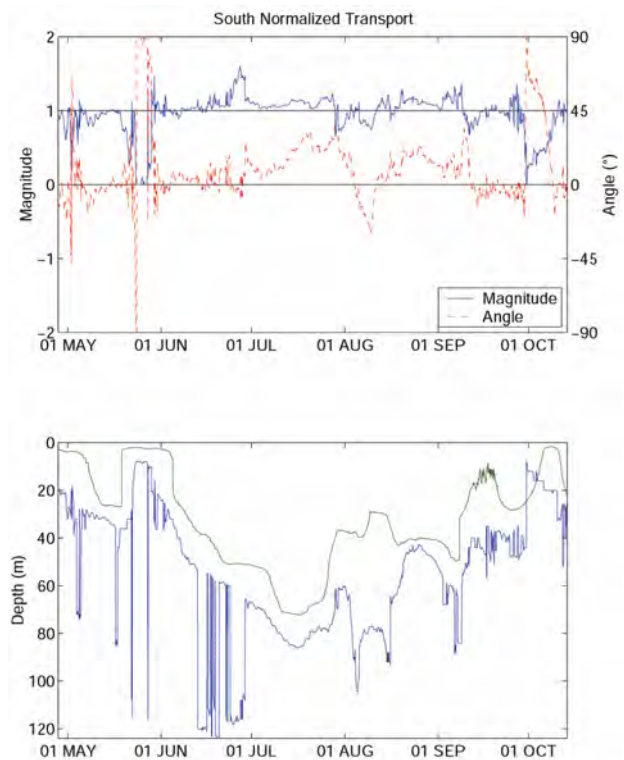


**Figure 9.** Penetration of wind-driven momentum during the SW Arabian Sea monsoon. As described in the text, currents are integrated to the depth at which observed transport is in best agreement with theoretical Ekman transport. (top) Magnitude (blue curve) and angle (red dashed curve) of observed transport relative to theory. (bottom) Penetration depth of observed wind-driven flow (blue curve) and mixed-layer depth (green curve) defined by a 0.1°C difference from the surface.

mixed layer shoals. Good agreement should be taken not as a test of the theory, but rather as proof that observations have resolved the wind-driven flow. The penetration depth of the wind-driven flow is correlated with, but consistently exceeds, the mixed-layer depth (measured by a  $0.1^\circ\text{C}$  difference from the surface). The penetration depth, while noisy, tends to be roughly 20 m deeper than the mixed-layer depth. The thickness of the sub-mixed-layer zone of turbulent momentum transfer seems not to be proportional to mixed-layer depth. Variations of the thickness of the sub-mixed-layer zone are perhaps weakly correlated with local stratification. In summary, the mixed layer is relevant to momentum transfer, but is not the whole story, as turbulence and stratification beneath the mixed layer matter.

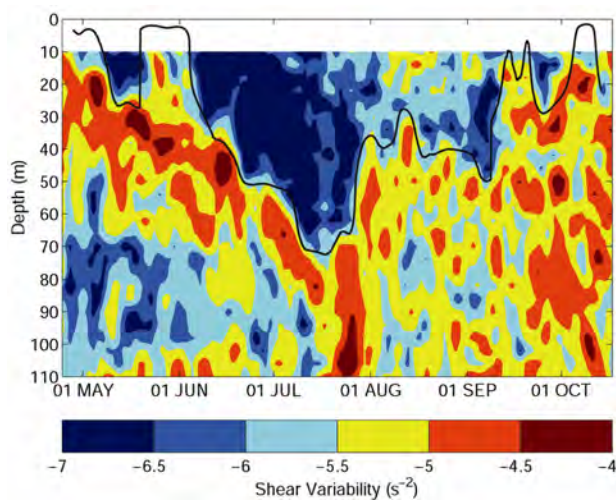


**Figure 10.** Near-inertial shear variability during the SW Arabian Sea monsoon. The black curve indicates the mixed layer depth. The mixed layer is relatively un-sheared relative to the region beneath.

Persistent shear is a distinguishing feature of the turbulent region just beneath the mixed layer, and the frequency content of this shear is dominantly near-inertial. The vertical distribution of near-inertial shear variability was calculated using wavelets for the Arabian sea data (Fig. 10). A region of high inertial shear lay beneath the mixed layer while it deepened during the SW monsoon. Shear was notably absent within the mixed layer, consistent with a slab. The monsoon in 1995 was remarkable for having a double onset (Flateau *et al.*, 2001); the monsoon turned on in early May, only to weaken in mid-May before moving on for good in early June. The weakening of the wind in mid-May was accompanied by restratification and

mixed-layer shoaling. However, the zone of high inertial shear was left behind. A later period of mixed-layer shoaling in late July was associated with an advective event, and further shoaling in September occurred when the monsoon ceased. Throughout these undulations the mixed layer remained relatively un-sheared, while inertial shear was energetic below.

The mixed-layer base is an important boundary, separating the slab-like mixed layer from the highly sheared region beneath. While turbulence does decay with depth, it does not disappear at the mixed-layer base, contrary to the traditional notion of the mixed-layer base as a boundary between quiescent and turbulent regions. In an effort to focus on this boundary, Weller and Plueddemann (1996) used a coordinate system fixed to the mixed-layer base (Fig. 11). They found inertial shear throughout the sub-mixed-layer ocean while subinertial shear was concentrated in a region just beneath the mixed layer. Analyses in a fixed coordinate system would smear this structure as the mixed layer shoals and deepens. Fixing the coordinate system to the mixed-layer base may be worthwhile in theoretical and modeling efforts, as well.

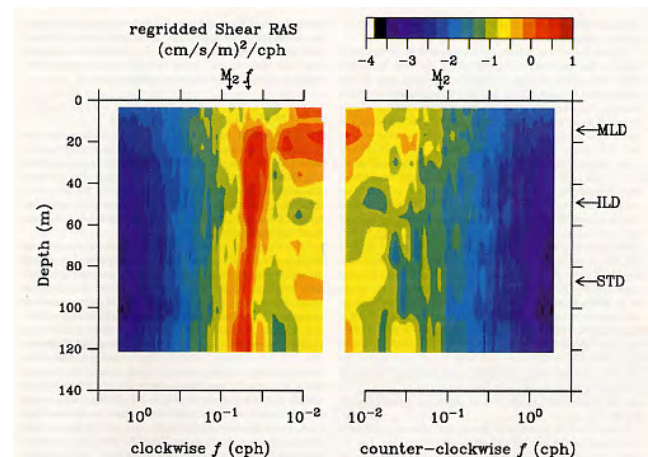


**Figure 11.** From Weller and Plueddemann (1996), the rotary autospectrum of shear plotted as a function of depth and frequency. The depth coordinate system follows the mixed-layer base denoted as “MLD” in the figure. Note the trapping of subinertial shear at the mixed-layer base.

## Conclusion

Ekman was correct in that there does exist a wind-forced velocity spiral. This spiral has been observed

over a wide range of time scales. Agreement with theoretical Ekman transport has indicated that observations and analyses have been successful at isolating the wind-driven flow. As Ekman predicted, stratification matters, as the observed spiral is flatter, and more slab-like than the theoretical spiral. Wind-driven momentum penetrates beneath the mixed-layer base into a turbulent region dominated by inertial shear. This sub-mixed-layer region is poorly understood, but critical to an accurate parameterization of momentum transfer in the upper ocean. An important topic for continued research is thus the stratified region just beneath the mixed layer.

**Acknowledgments.** All of the experiments reviewed here were supported by the Office of Naval Research, whose past funding has been crucial to the study of upper ocean processes. I thank Chris Garrett and Peter Müller for their gracious invitation to the Aha Hulikoa meeting. During the preparation of this article, I was supported by the National Science Foundation under grants OCE-0002598, OCE-9819521, and OCE-9819530.

## References

- Chereskin, T.K., Direct evidence for an Ekman balance in the California Current, *J. Geophys. Res.*, *100* (C9), 18,261-18,269, 1995.
- Chereskin, T.K., and D. Roemmich, A comparison of measured and wind-derived Ekman transport at 11°N in the Atlantic Ocean, *J. Phys. Oceanogr.*, *21* (6), 869-878, 1991.
- Davis, R.E., R. de Szoeke, D. Halpern, and P. Niiler, Variability in the upper ocean during MILE. Part I: The heat and momentum balances, *Deep-Sea Res.*, *28*, 1427-1452, 1981a.
- Davis, R.E., R. de Szoeke, and P. Niiler, Variability in the upper ocean during MILE. Part II: Modelling the mixed layer response, *Deep-Sea Res.*, *28*, 1453-1475, 1981b.
- Ekman, V.W., On the influence of the earth's rotation on ocean currents, *Ark. Mat. Astron. Fys.*, *2* (11), 1-52, 1905.
- Flatau, M.K., P.J. Flatau, and D. Rudnick, The dynamics of double monsoon onsets, *J. Climate*, *14*, 4130-4146, 2001.
- Hunkins, K., Ekman drift currents in the Arctic Ocean, *Deep-Sea Res.*, *13*, 607-620, 1966.
- Munk, W., The evolution of physical oceanography in the last hundred years, *Oceanography*, *15* (1), 135-141, 2002.
- Niiler, P.P., Deepening of the wind-mixed layer, *J. Mar. Res.*, *33*, 405-422, 1975.
- Philander, S.G.H., Forced oceanic waves, *Rev. Geophys. Space Phys.*, *16*, 15-46, 1978.
- Price, J.F., R.A. Weller, and R. Pinkel, Diurnal cycling: Observations and models of the upper ocean response to diurnal heating, cooling, and wind mixing, *J. Geophys. Res.*, *91* (C7), 8411-8427, 1986.
- Price, J.F., R.A. Weller, and R.R. Schudlich, Wind-driven ocean currents and Ekman transport, *Science*, *238*, 1534-1538, 1987.
- Rudnick, D.L., and R.A. Weller, Observations of superinertial and near-inertial wind-driven flow, *J. Phys. Oceanogr.*, *23* (11), 2351-2359, 1993.
- Weller, R.A., and R.E. Davis, A vector-measuring current meter, *Deep-Sea Res.*, *27*, 565-582, 1980.
- Weller, R.A., A.S. Fischer, D.L. Rudnick, C.E. Eriksen, T.D. Dickey, J. Marra, C. Fox, and R. Leben, Moored observations of upper ocean response to the monsoon in the Arabian Sea during 1994-1995, *Deep-Sea Res. II*, *49*, 2231-2264, 2002.
- Weller, R.A., and A.J. Plueddemann, Observations of the vertical structure of the oceanic boundary layer, *J. Geophys. Res.*, *101*, 8789-8806, 1996.
- Weller, R.A., D.L. Rudnick, C.C. Eriksen, K.L. Polzin, N.S. Oakey, J.W. Toole, R.W. Schmitt, and R.T. Pollard, Forced ocean response during the Frontal Air-Sea Interaction Experiment, *J. Geophys. Res.*, *96* (C5), 8611-8638, 1991.